Modelling and simulation of a bio-mimetic underwater robot inspired by feather sea star using smart actuators

Anitha Francis, V.K.Gupta, Sujoy Mukherjee

Abstract

Many kinds of underwater robots were developed in recent years. Modelling and simulation of a bio-mimetic underwater robot, which is inspired by Antedon Petasus (scientific name of Feather Sea Star) is introduced in this paper. This underwater robot finds its own application in small spaces and congested environment. The configuration and the propulsion nature of feather sea star are analysed. The simple design which mimics the organism using smart actuators like Shape Memory Alloy (SMA) and Ionic Polymer Metallic Composite (IPMC) has been proposed. As robot should survive in underwater environment, consideration of hydrodynamic effects is very important, especially the drag force consideration. The design has been modelled in SOLIDWORKS and its effective analysis has been carried out in a sophisticated underwater environment provided by ANSYS-Fluent. The flapping module of IPMC is used for actuating and manoeuvring. The shape memory alloy is used to achieve the proper propulsion. The calculated theoretical value and the simulated value of drag co-efficient are compared. The effects of hydrodynamics on the bot have also been calculated.

Keywords: Smart actuators, Shape memory alloy, Ionic polymer metallic composites, Biomimetic underwater robot, SOLIDWORKS model, ANSYS-Fluent.

1 Introduction

Maritime investigation without human intercession is considered essential because of its resources and it would be a challenge for human being to withstand the harsh oceanic surroundings. So, it becomes an emerging field of robotic research [3]. Recently, numerous scientists demonstrate their enthusiasm of creating biomimetic underwater robots. This paper presents the design and development of a biomimetic underwater robot inspired by the species called Feather Sea Star. Soft links and light-weight structure are required to develop the robot for mimicking this organism. Robot using Shape Memory Alloy (SMA) and Ionic Polymer Metallic Composite (IPMC) instead servomotors as actuators had been tried. As robot should survive in underwater environment, consideration of hydrodynamic effects is very important, especially the drag force consideration. Estimation of drag force co-efficient can be done either experimenting on real-time basis (i.e.) having a water tank setup and letting the robot into it or simulating the model of the robot in underwater environment. As simulation is cost-effective and would take less time, it would be considered for estimation of drag force co-efficient. The design of the robot is modeled in SOLIDWORKS and the effective analysis in underwater environment is done in ANSYS-Fluent.

A biomimetic robot fish had been designed, fabricated and analysed by Donya et al in 2008 [8]. Xiu et al proposed a new driving mechanism of a jellyfish robot using SMA and IPMC [6]. Here SMA is used with a light-weight spring for achieving contraction and relaxation for jet propulsion and IPMC is used for changing the direction of actuation. The SMA has been mathematically modelled in new direction and proper control had been achieved by Jayendar et al [12]. Two controllers had been developed and implemented experimentally based on the model. Their simulation and experimental results had been analysed in different mediums. The uniqueness of their cryogenic properties had been revealed. Their potential of being a cryogenic sensor or actuator had been analysed. The resistance of IPMC increase with decreasing temperature and it is a property, opposite to all metallic conductors. In 2004, using neural network, the position of the shape memory alloy had been controlled by Ma et al [13]. Carangiform swimming mode had been adopted for this fish-robot and its 2D model had been analysed in ANSYS-Fluent besides the test results of actual robot. Won et al had reviewed biomimetic underwater robots which use smart actuators [15]. Different smart actuators can be utilized for biomimetic underwater robot, so the difference in their efficiencies to propel, speed of actuation, environmental constraints had been explained well with suitable graphs and

Anitha Francis
Mechatronics, Indian Institute of Information Technology, Design and Manufacturing (IIITDM) – Jabalpur, E-mail: anitha.francis@iiitdmj.ac.in

Vijay Kumar Gupta
Mechatronics, Dean Academics, Indian Institute of Information Technology, Design and Manufacturing (IIITDM) – Jabalpur, E-mail: vkgupta@iiitdmj.ac.in

Sujoy Mukherjee
Mechanical, Indian Institute of Information Technology, Design and Manufacturing (IIITDM) – Jabalpur, E-mail: sujoy@iiitdmj.ac.in

tables. Shahinpoor et al reviewed IPMC as a sensor, actuator and artificial muscle in 1998 [16]. The electrical resistance feedback control had been proposed and implemented to control the spring shaped SMA, so as to achieve proper position regulation of the material. A worm-like robot, using IPMC had been modelled, fabricated and controlled by Paola et al [18]. This is an autonomous robot which mimics ray fish and made use of IPMC for their energy efficient locomotion. A two motion at different attitudes of an underwater robot using IPMC and SMA had been proposed in the year 2012 by Liwei et al [20]. In his paper, the use of the same IPMC as both leg and caudal fin in single application had been proposed and implemented efficiently. The worm-like robot uses cellular neural network for their controlled actuation of the skeleton which is made of IPMC. A rajiform swimming robot had been developed by Kentaro et al [23]. Fish inspired biomimetic propulsion using IPMC has been discussed by Karthigan et al [24]. Numerical simulation had been done to analyse three different flapping pectoral fin made of IPMC which imitates three different Labridae fish species.

2 Methodology

The performance of different smart materials in accordance with stress-strain ratio involving actuation energy density had been analyzed. Materials like Shape Memory Alloy (SMA) and Ionic Polymer Metallic Composite (IPMC) with respect to the stress-strain ratio, found suitable to be used as smart actuators for the bot for jet propulsion. The steps involved for the drag co-efficient estimation of this bot using smart actuators had been presented with the help of the following flowchart:

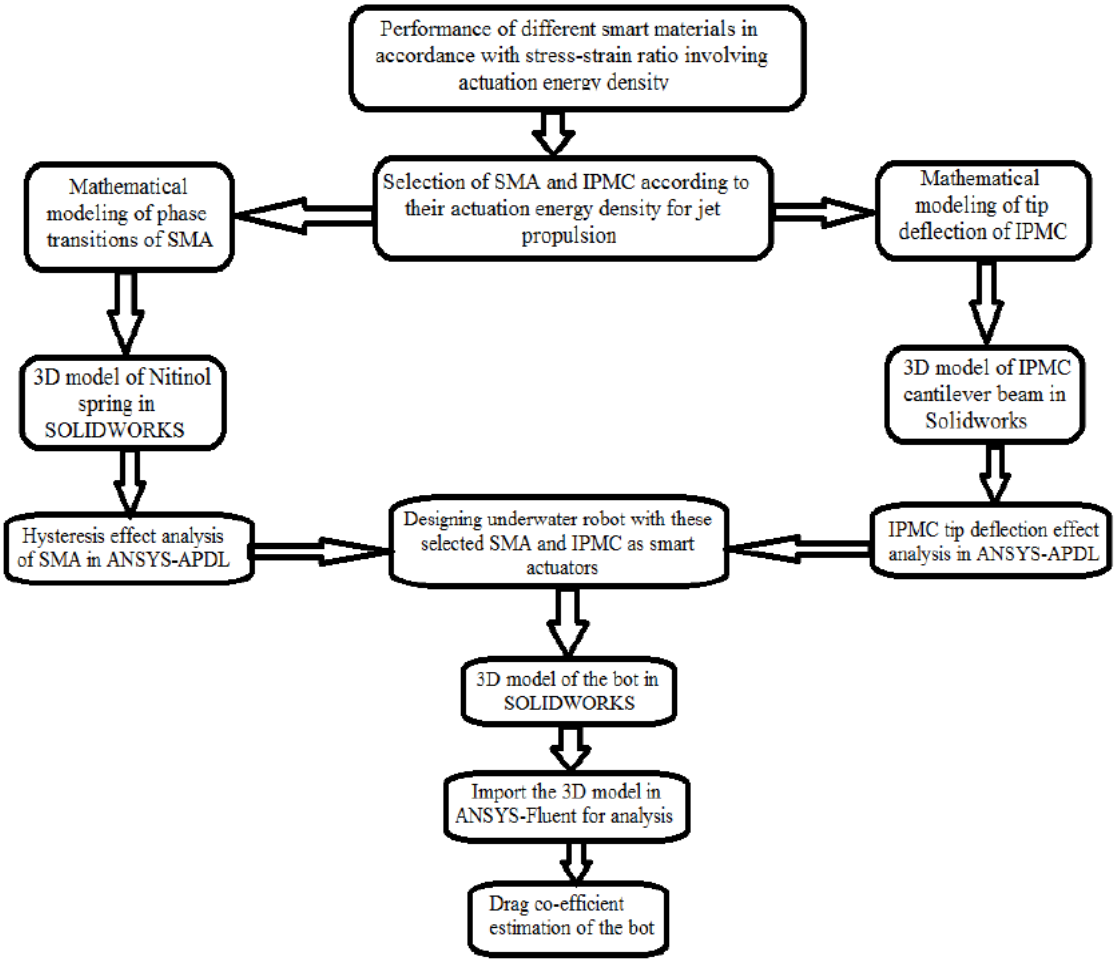

Figure 1: Flowchart of the methodology

3 Design

3.1 SMA Modeling

The SMA used as an actuator of the proposed robot is a nitinol spring which is shown in figure 2. The spring is about 20mm long originally at it retains to its originality at about 40-45 degree Celsius, under any external deformations. It can be deformed unto 150mm. The spring has 21 windings, its wire diameter is 0.75mm and spring‘s outer diameter is 6mm. With these specifications, the nitinol spring had been modeled in SOLIDWORKS as a 3D model (figure 2).

Figure 2: SOLIDWORKS model of nitinol spring

The 3D model had been further imported in ANSYS – APDL as shown in figure 3. Setting the properties like modulus of austenite and marten-site elements, their hardening parameters, reference temperatures, elastic limit, maximum transformation strain upon compression and tension loading and unloading. The plot of total strain versus stress had been obtained as result which is shown in figure 4, represents its hysteresis effect.

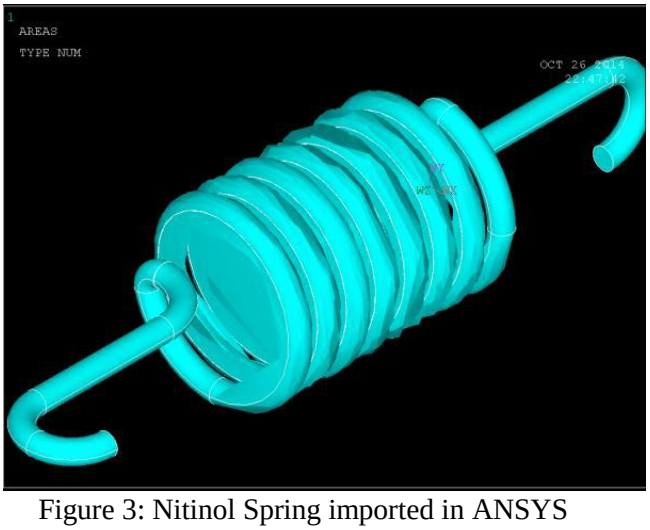

Figure 3: Nitinol Spring imported in ANSYS

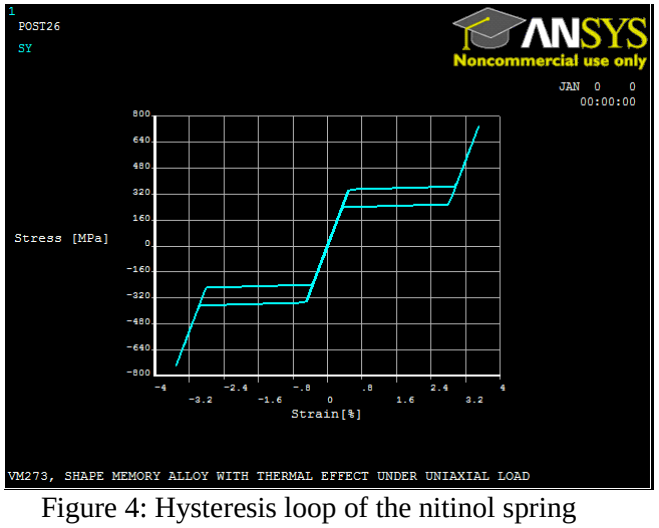

Figure 4: Hysteresis loop of the nitinol spring

The hysteresis loop obtained as result, explains the proposed nitinol spring‘s properties and its loading and unloading effects.

3.2 IPMC Modeling

The flapping module of IPMC pair of about 7cm is used as an actuator. Its thickness is about 12 μm. When electrical supply is given to it in the order of 1.5V, it deforms and the deformation span is about 10cm as shown in figure 5 and 6.

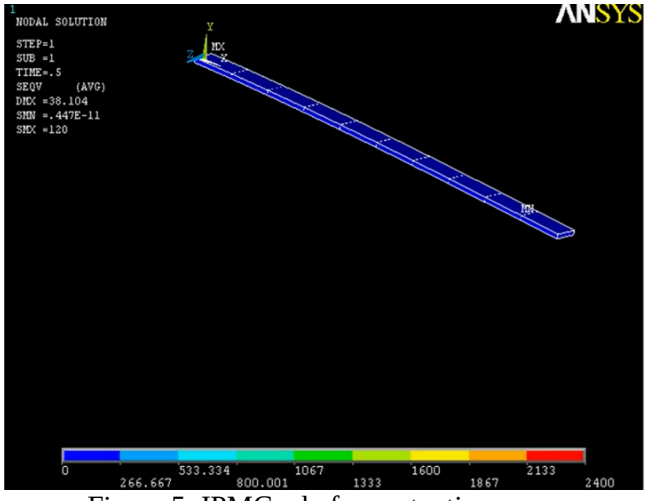

Figure 5: IPMC – before actuation

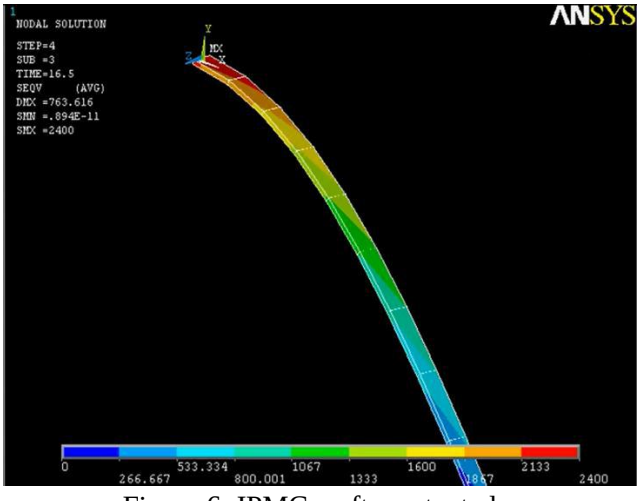

Figure 6: IPMC – after actuated

One of them was modeled as a cantilever beam to find its deflection graphically in ANSYS. The 3D 8-node structural solid element is used to model the IPMC and the deformation is obtained in air. The material properties used for analysis is given in table 1.

Table 1: Material properties of IPMC used

S.no	Parameters	Values
1	Density	1.25 g/cc
2	Young's modulus	280 MPa
3	Poisson Ratio	0.487
4	Viscous damping co-efficient	0.37

3.3 Actual Design of the Robot

As it can be seen from the literature that several researches have used the hybrid modelling approach for the development of underwater robot[6]. The body is designed like bell – shape and it is made up of very light-weight latex, the SMA is placed at its centre through hooks with latex. The latex material is sandwiched between hooks (placed inside) and IPMC

Figure 7: 3D model indicating SMA

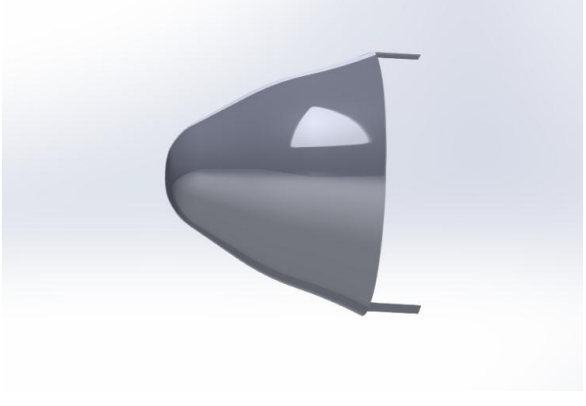

Figure 8: 3D model indicating IPMC

(attached outside).

The design is modeled in SOLIDWORKS with the SMA 20mm length (before deformation) and other specifications of SMA were discussed earlier, bell height is 30mm. As IPMC is actuated, they tend to pull latex and mechanical deformation occurs in SMA, then later it is to be programmed to give supply to SMA, so as it regain to its original shape. Likewise, the bell enlarges and water enters in and then after electrical supply is given to SMA the bell contracts. This expansion and contraction paves way to jet propulsion.

4 Ansys analysis:

The 3D SOLIDWORKS model is then imported in ANSYS workbench – geometry, to proceed further for ANSYS-Fluent solutions. The 3D geometry is then enclosed by a cylinder enclosure as a flow field which is comparatively large enough to analyze the bot‘s behavior in it. The usual steps are followed here for further hydrodynamic analysis in ANSYS-Fluent.

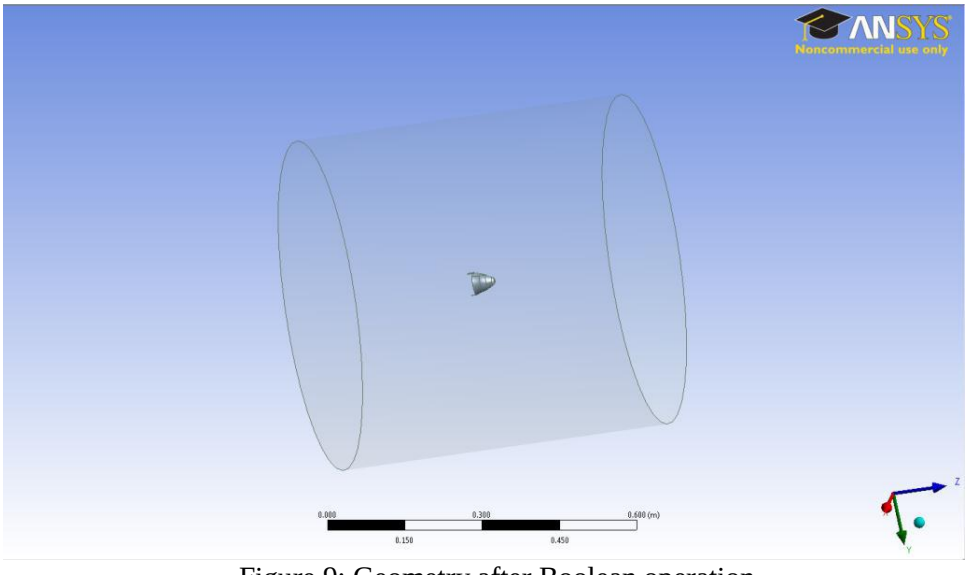

Figure 9: Geometry after Boolean operation

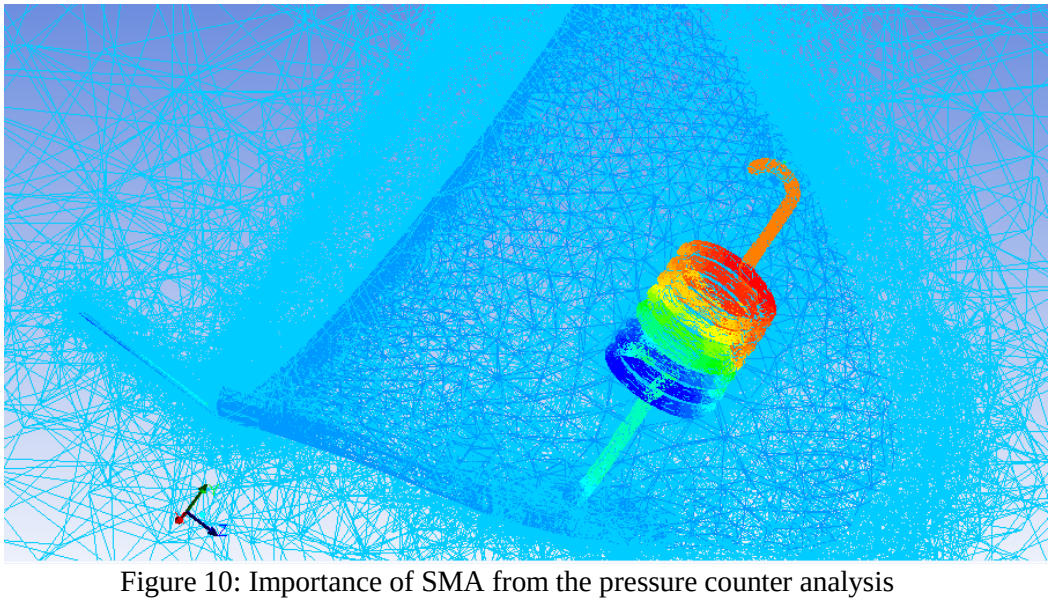

Figure 10: Importance of SMA from the pressure counter analysis

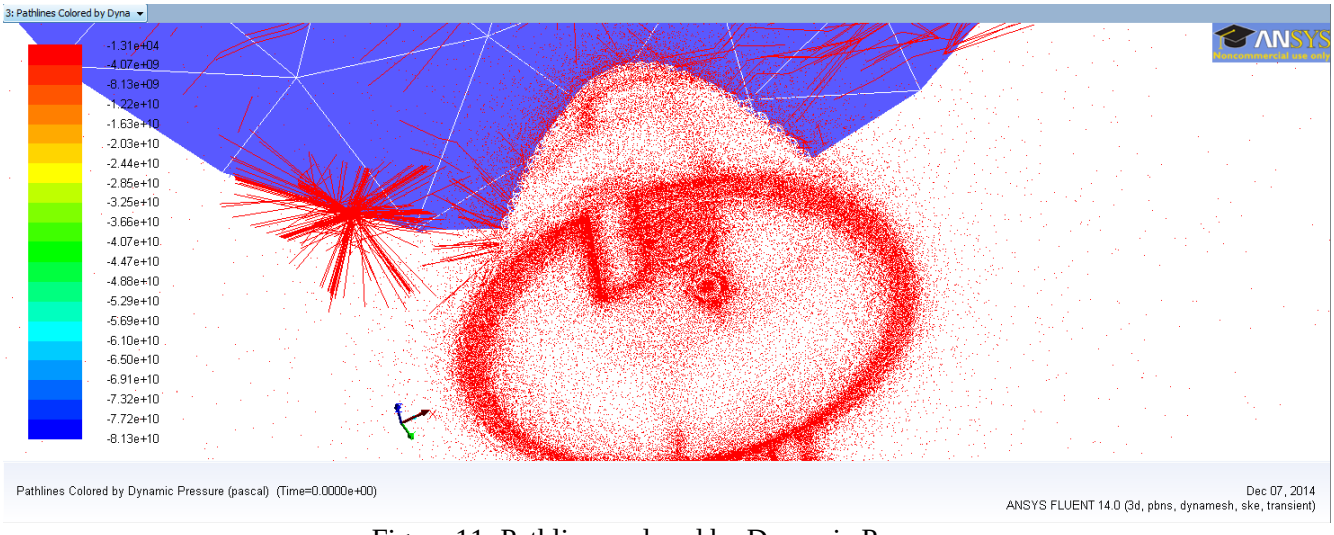

Figure 11: Pathlines colored by Dynamic Pressure

The inlet velocity condition, pressure condition for outlet and the symmetry condition for wall had been applied. Then, after subtracting the 3D geometry with the cylinder-pipe enclosure, by applying Boolean function, the geometry had been meshed properly with about 2.5 lakh mesh cells. This geometry after Boolean operation is shown in Figure 9. The importance of SMA for actuation is demonstrated from the pressure counter analysis is shown in Figure 10. Figure 11 illustrates the pathlines colored by dynamic pressure. The convergence graph after setting the boundary conditions is shown in Figure 12.

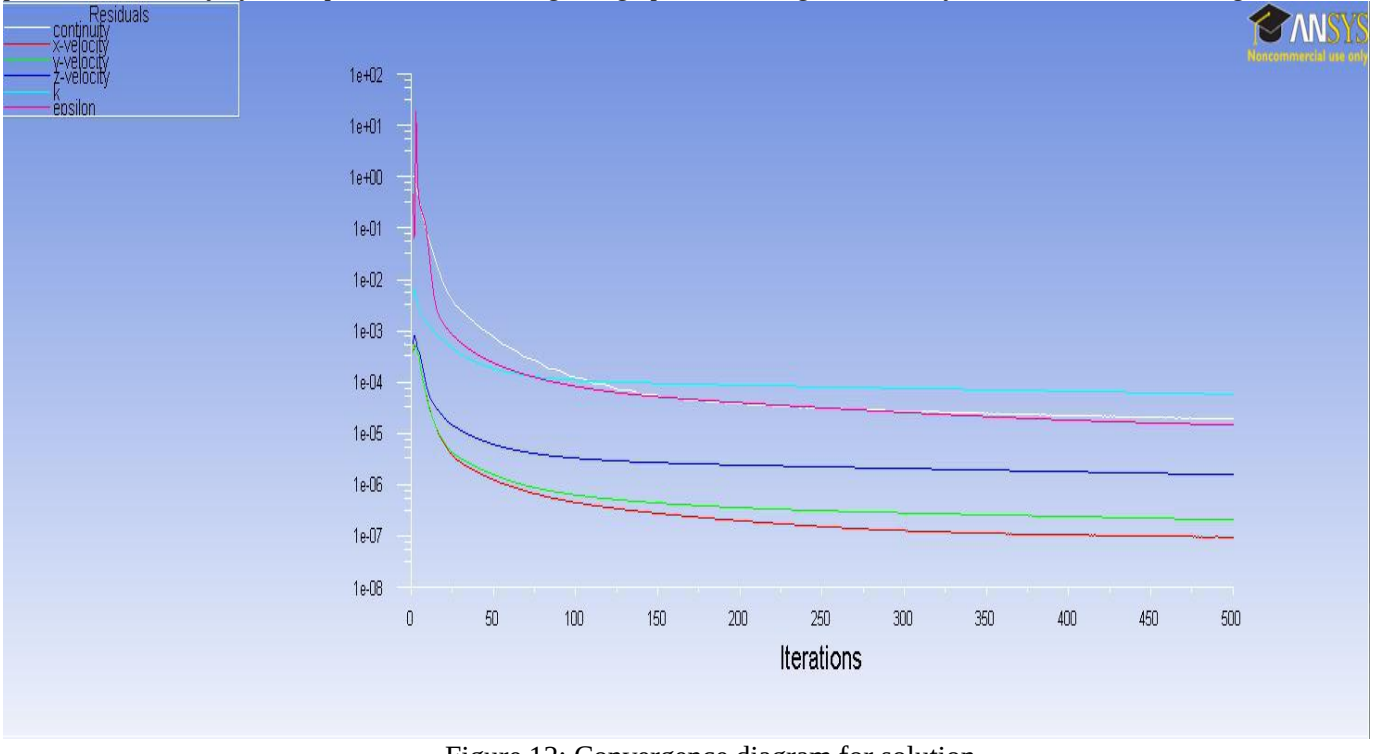

Figure 12: Convergence diagram for solution

5 Results and Observations

The obtained pressure counter diagram as shown in Figure 13 concludes that, the SMA spring and IPMC fin is unavoidable for the propulsion, the dark blue color indicates the high speed part. The counters of static pressure with pressure counter coding, where dynamic mesh is adopted and transient effect is checked. The different colors provided to the smart materials indicate their importance in propulsion of the design. The red and orange colored parts act according to the pressure provided, so in these parts, the effect of hydrodynamics is high. Irrespective to the surrounding, the dark blue colored part indicates the

high speed operation. As IPMC works effectively in water surrounding, its high speed nature is not affected by the hydrodynamics effect. This pressure counter diagram is shown in figure 13. The robot is considered to move in vertical direction (with the cylinder vertically placed), and its drag force co-efficient is found to be 0.8867. The hydrodynamic features of the robot are deducted from the velocity vector, pressure contours and the drag co-efficient estimation graph.

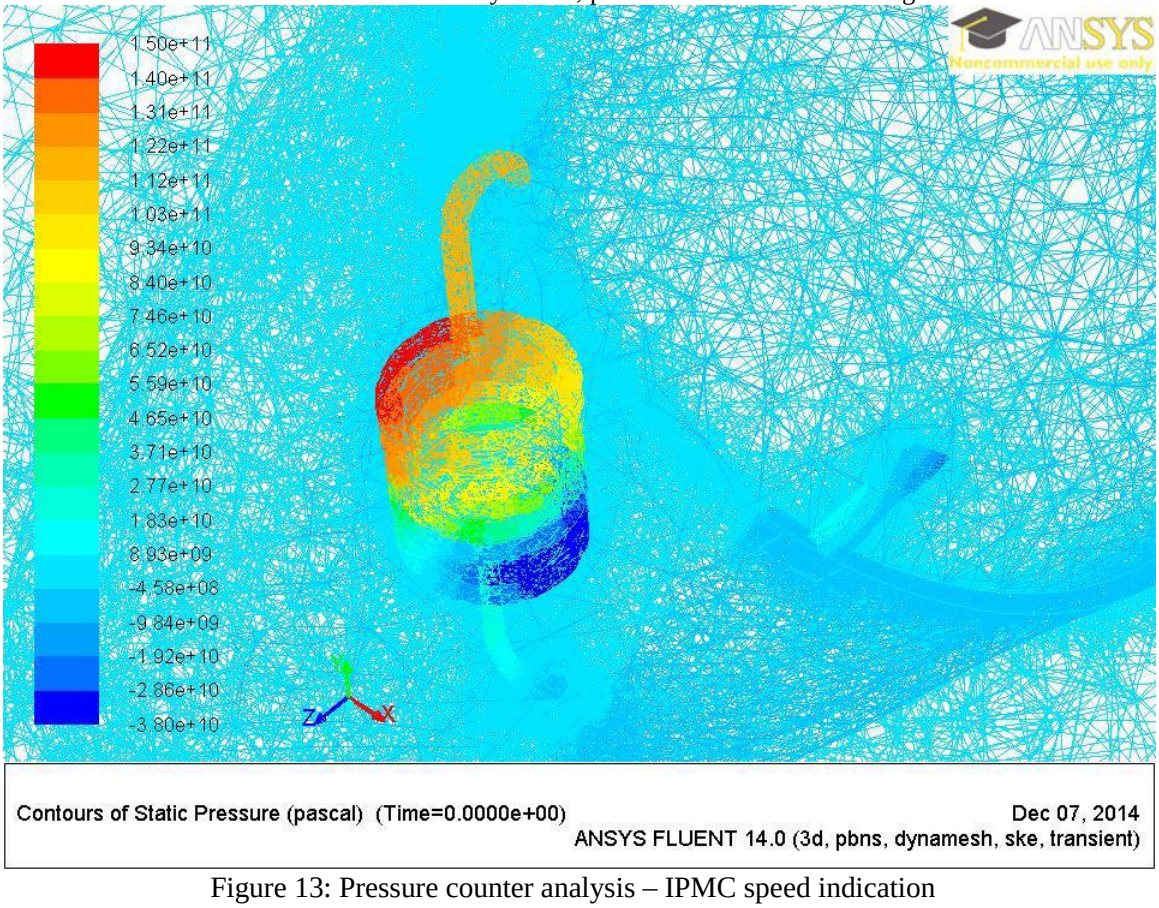

Figure 13: Pressure counter analysis – IPMC speed indication

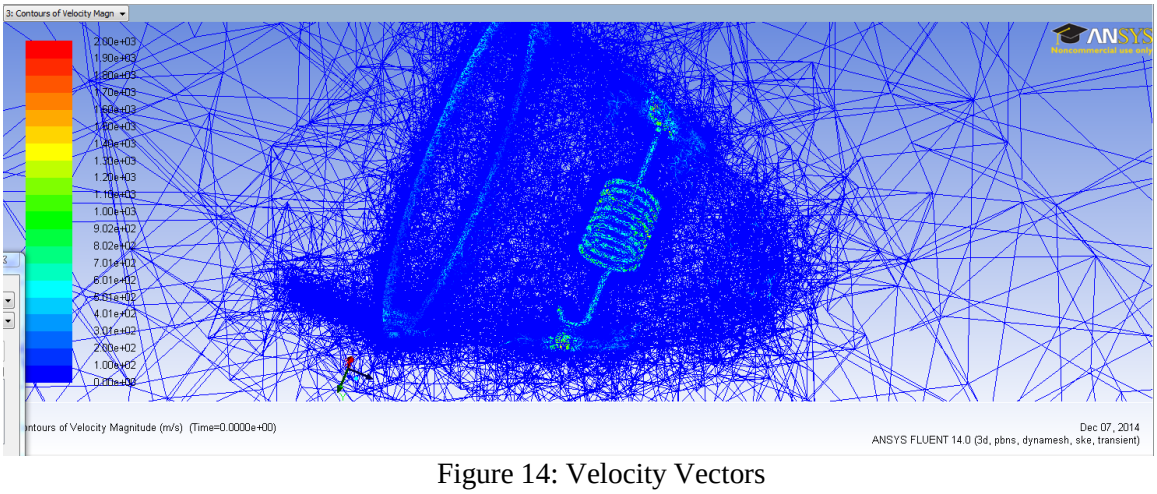

Figure 14: Velocity Vectors

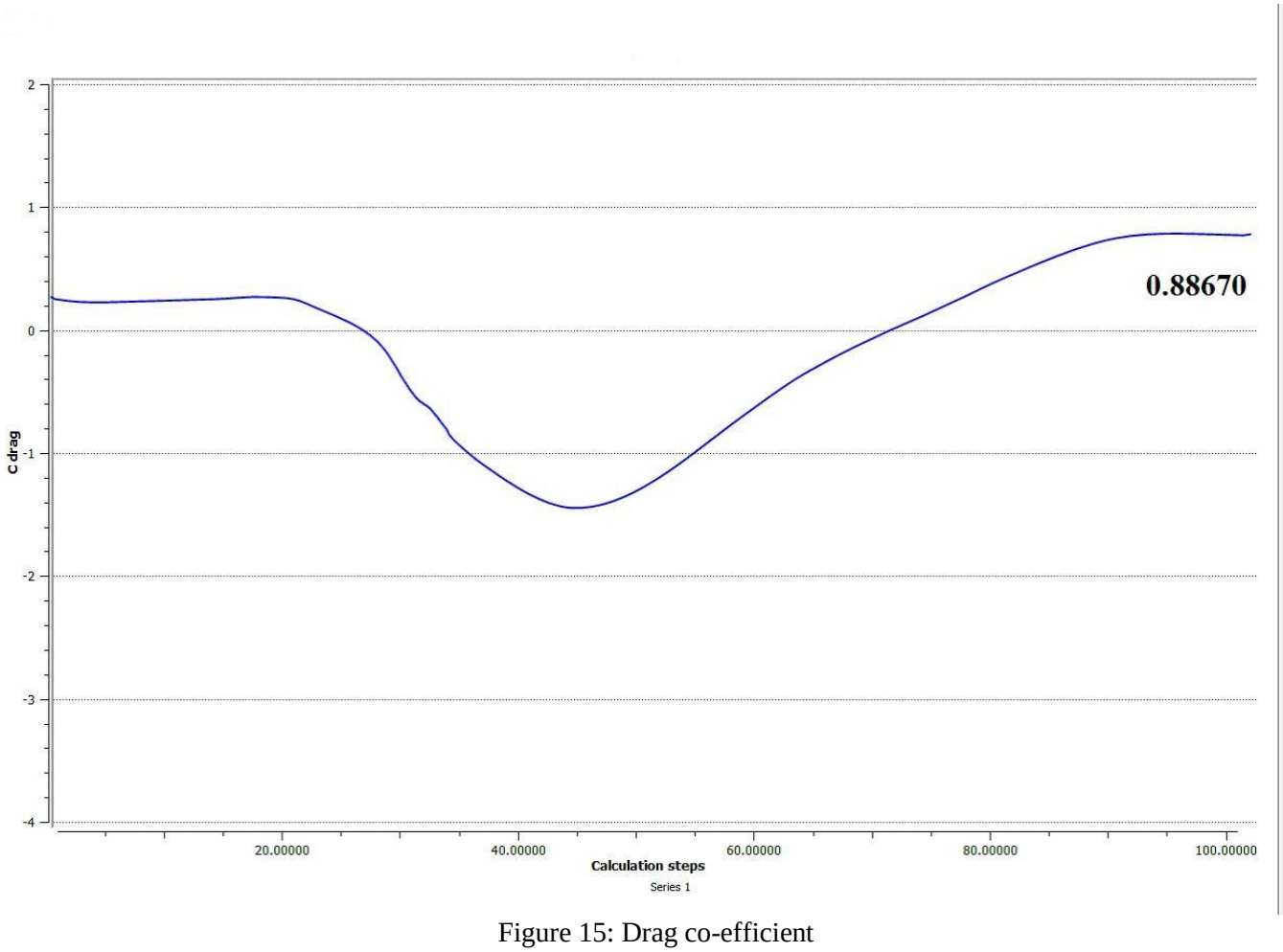

Figure 15: Drag co-efficient

As mentioned, after the numerical solution of drag co-efficient and the drag co-efficient estimation from the ANSYS-Fluent analysis (the result of which is shown in Figure 15) suffers from only 2.7% error which is negligible [Appendix I]. So, it is observed from the analysis result that the water provides larger resistance for this bot and eventually the drag force will be high.

6 Conclusions

The design had been made up of smart materials like SMA and IPMC, which also mimics the propulsion of the organism by contraction and relaxation using SMA and IPMC. It had also been modelled in SOLIDWORKS for analysis and the drag co-efficient obtained in analysis is 0.88670. If the same constraints as the design made with springs and servomotor which has 0.47862 drag co-efficient, had been applied, the drag force will be high for this design and can be proved for better mimicking of the organism.

7 References

[1] M.Triantafyllou, G.Triantafyllou, ―An Efficient Swimming Machine‖, Scientic American, 1995, 272(3), pp64-70.
[2] A.J.Ijspreet, J.Hallam and D.Willshaw, ―Evolving swimming controllers for a simulated lamprey with inspiration from neurobiology‖. Adaptive behavior, 7(2):151-172, 1999.
[3] A.J.Ijspreet, A.Crespi, D.ryczko and JM.Cabelguen, ―From swimming to walking with a salamander robot driven by a spinal cart model‖. Science, 315:1416-1420, 2007.
[4] Underwater vehicles and National meets‖, National academy press, 1996. Accession number: 1204. Publication type: eBook. Language: English.

[5] Donya Mohammadshahi, Aghil Yousefi-koma, Shahnaz Bahmanyar, Hassan Ghassemi, Hessam Maleki, ―Design, Fabrication and Hydrodynamic analysis of a Biomimetic Robot Fish‖. International Journal of Mechanics, Issue 4, Volume 2, 2008
[6]Xiu Fen.Ye, Ya Nam.Hu, Shu Xiang Guo, Yu Dong.Su, "Driving mechanism of a new jellyfish like microrobot". Proceedings of 2008 IEEE International conference on Mechatronics and Automation, August 5-8, 2008, Takamatsu, Japan.
[7] Shalvlb Nir, Shovel Shraga, Boaz Ben Moshe, Igor Ruchaevski, Tamir Shteinberg. ―A jellyfish like robot mimicking jet propulsion‖. IEEE 27th convention of Electrical and Electronics Engineering,2012.
[8] FESTO. Bionic learning network: Inspired by nature (Press release No. TC 06/08), 21 April 2008.
[9] Gianluca Antonelli, ―Underwater Robots Motion and Force Control of Vehicle-Manipulator Systems‖, Springer-Verlag Berlin Heidelberg, 2003.
[10] Irfan Abd Rahman, Surina Mat Suboh, Mohd Rizal Arshad, ―Theory and Design Issues of Underwater Manipulator‖, International Conference on Control, Instrumentation and Mechatronics Engineering (CIM'07), Malaysia, May 28-29,2007.
[11]Kaan Divringi, Can Ozcan, ―Advanced Shape Memory Alloy Material Models for ANSYS‖. Ozen Engineering Inc.
[12]J.Jayendar, R.V.Patel,S.Nikumb, M.Ostojic, ―Modeling and control of Shape Memory Alloy Actuators‖. IEEE transactions on Control systems technology, VOL: 16, NO.2, March 2008.
[13]N.Ma, G.Song and H-J.Lee, ―Position control of shape memory alloy actuators with internal electrical resistance feedback using neural networks. Smart Mater.Struct. 13 (2004) 777–783 PII: S0964-1726(04)77382-6.
[14]Donya Mohammadshahi, Aghil Yousefi-koma, Shahnaz Bahmanyar, Hassan Ghassemi, Hessam Maleki, ―Design, Fabrication and Hydrodynamic analysis of a Biomimetic Robot Fish‖. International Journal of Mechanics, Issue 4, Volume 2, 2008.
[15]Won-Shik Chu, Kyung-Tae Lee1, Sung-Hyuk Song, Min-Woo Han, Jang Yeob Lee, Hyung-Soo Kim, Min-Soo Kim, Yong-Jai Park, Kyu-Jin Cho and Sung-Hoon Ahn, ―Review of Biomimetic Underwater Robots Using Smart Actuators‖. international journal of precision engineering and manufacturing Vol. 13, No. 7, pp. 1281-1292, July 2012.
[16]M. Shahinpoor,Y . Bar-Cohen, J, .O. Simpson and J. Smith, "Ionic Polymer-MetalComposites (IPMC) As Biomimetic Sensors, Actuators & Artificial Muscles- A Review", J. of smart materials, 1998.
[17]Simson T. Wilson, Sudheer A.P, Santhakumar Mohan,―Dynamic Modeling, Simulation and Spatial Control of an Underwater Robot Equipped with a Planar Manipulator‖. IEEE,2011.
[18]Paolo Arena, Claudia Bonomo, Luigi Fortuna, Mattia Frasca and Salvatore Graziani, "Design and Control of an IPMC Wormlike Robot", IEEE Transactions on systems, man, and cybernetics—part b: cybernetics, vol. 36, no. 5, October 2006.
[19]Michael Griebel, Thomas Dornseifer, Tilman Neunhoeffer, "Numerical Simulation in Fluid Dynamics". Society for Industrial and Applied mathematics, Philadelphia, 1998.
[20]Liwei Shi, Shuxiang Guo, Maoxun Li, Shilian Mao, Nan Xiao, Baofeng Gao, Zhibin Song and Kinji Asaka, "A Novel Soft Biomimetic Microrobot with Two Motion Attitudes", *Sensors* 2012, ISSN 1424-8220**,** www.mdpi.com/journal/sensors.
[21]Cheng Chin, Michael Lau, "Modeling and Testing of Hydrodynamic Damping Model for a Complex-shaped Remotely-operated Vehicle for Control". J. Marine Sci. Appl. (2012) 11: 150-163.
[22]Kuan M.Tan, Tien-Fu Lu, Amir Anvar, "Drag Coefficient Estimation Model to Simulate Dynamic Control of Autonomous Underwater Vehicle (AUV) Motion". 20th International Congress on Modeling and Simulation, Adelaide, Australia, 1–6 December 2013.
[23]Kentaro Takagi, Masanori Yamamura, Zhi-Wei Luo, Masaki Onishi, Shinya Hirano, Kinji Asaka, Yoshikazu Hayakawa, "Development of a Rajiform Swimming Robot using Ionic Polymer Artificial Muscles", Proceedings of the 2006 IEEE/RSJ International Conference on Intelligent Robots and Systems October 9 - 15, 2006, Beijing, China.
[24]G. Karthigan, Sujoy Mukherjee, Ranjan Ganguli, "Fish Inspired Biomimetic Ionic Polymer Metal Composite Pectoral Fins Using *Labriform* Propulsion". Proceedings of the ASME 2011 Conference on Smart Materials, Adaptive Structures and Intelligent Systems. SMASIS2011, September 18-21, 2011, Phoenix, Arizona, USA.
[25]Ashitava Ghosal, "Robotics, Fundamental concepts and analysis", Oxford university press, 2006.
[26]S.K.Som, Gautam Biswas, Suman Chakraborty, "Introduction to fluid mechanics and fluid machines", third edition, McGraw Hill, 2012.
[27]Gu, Petkov and Konstantinov, "Robust control design with MATLAB", Springer, 2005.
[28]Frank.M.White, "Fluid Mechanics", fifth edition, McGraw Hill, 2003.

Appendix I

Mathematical solution for drag co-efficient

It is harder to break down numerical models utilizing the exact partial differential equations and it is necessary that the continuous system be discretized to a finite–dimensional system. Here, finite element method (FEM) is utilized to discretize a continuous system. One of the key contrasts in the middle of rigid and flexible manipulators is the strain energy in the

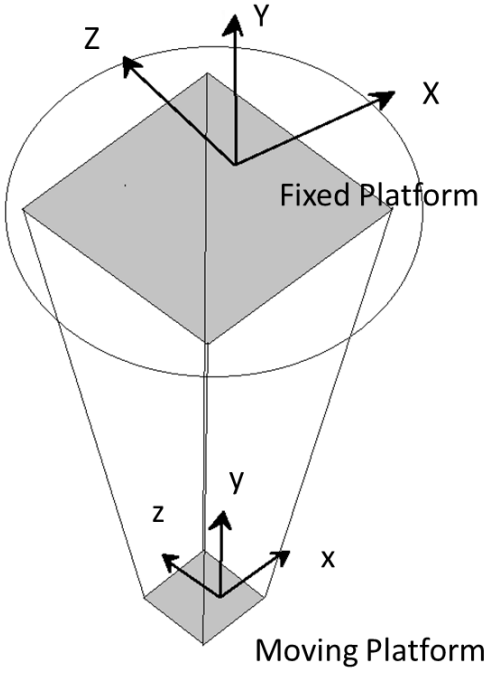

Figure 16: Free body diagram of the bot

vibrating link, which must be considered in evaluating the potential energy of the system. The kinematic modeling of this flexible manipulator is completed with the supposition that flexible deformations are little and linear elasticity equations are utilized. For kinematic and dynamic analysis, it can be graphically represented as in the figure 16.

The mathematical model is similar to the spatial 3-DOF parallel manipulator. The suspended maintaining so as to the moving platform had been compelled strain which ends in sets at the vertices of fixed platform. Position and orientation of the moving platform had been dictated by winches which independently control every link.

A platform is appended toward the end of the linear links. Let the centroid (centre point of the moving actuator) be "p" and the focal point of the platform be called as 'base'. The position vector is given as follows,

$$^{base}p = (¼)*(^{base}S_1 + ^{base}S_2 + ^{base}S_3 + ^{base}S_4) \text{ ----------(1)}$$

The moving platform's orientation would be known, once the position vectors are referred to, which had been solved as

$$^{base}[R]_{top} = \begin{matrix} 0.7869 & 0.5329 & -0.0506 \\ -0.4280 & 0.8602 & 0.4121 \\ 0.2529 & -0.2720 & 0.9502 \end{matrix}$$

----------(2)

Recursive algorithm is utilized to calculate the dynamics for foreseeing the system as a part of parallel system. Utilizing loop-closure constraint equations, the passive joint variables cannot be neglected.

While computing the dynamics, forces of the links were analysed and along these links the forward force experienced in "y" direction (as vertical direction of propulsion is considered) figured as,

$$F_y = 127mN \text{ ----------} \quad \textbf{(3)}$$

This force would be considered as the drag force and the drag co-efficient is given by,

$$C_d = 2F_y / \rho V^2 A \text{ ----------} \quad \textbf{(4)}$$

As the relative velocity 'V' is 65mm/s, ρ – the density of water is 1000 kg/m^3 and frontal area of the bot is 0.144m^2. Hence, the drag co-efficient (C_d) calculated theoretically is 0.8627591.

Appendix II

Modeling of Shape Memory Alloys

Nitinol is an alloy of Nickel and Titanium, which is a common shape memory alloy. Because of its thermo-mechanical properties, it can also be called as smart alloy, muscle wire, memory alloy, memory metal, smart metal, etc. This shape memory alloy is a solid state alternative to conventional actuators such as pneumatic, hydraulic and motor based systems. The phases of the nitinol, corresponds to the configuration of nickel and titanium in the crystal structure. So, nitinol can

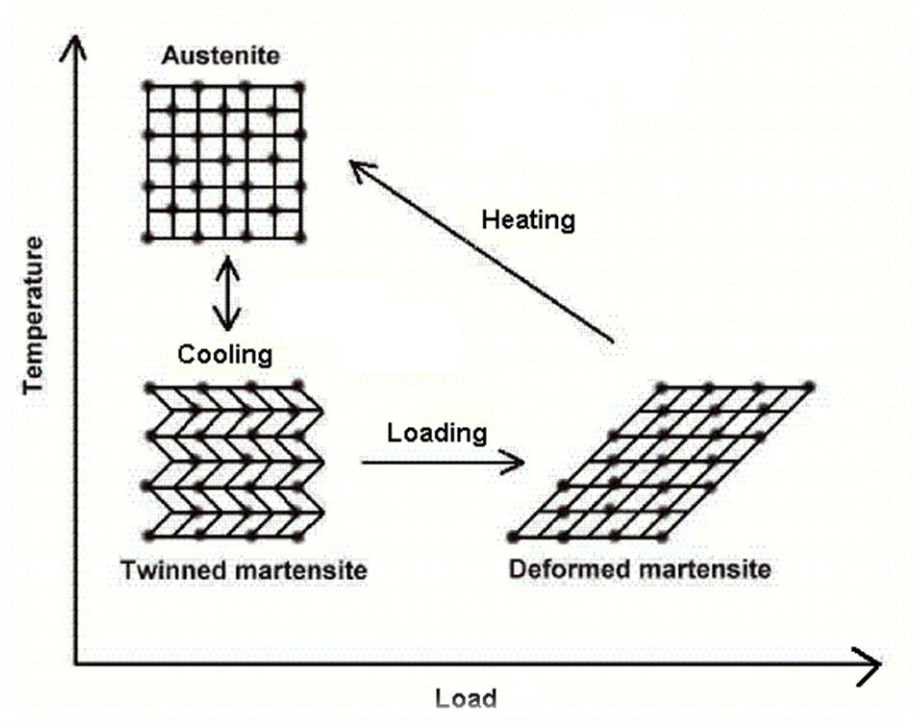

Figure 18: Shape Memory Effects

exists in two different phases known as, austenite and marten-site; and in three different crystal structures – austenite, twinned marten-site and de-twinned marten-site. The nitinol structure will be stiff, when it is at its austenite phase which occurs at higher temperatures. The deformation occurred in the material can be recoverable to some extent with respect to the material's strain property. As said, in marten-site phase the material will be less stiff, which will be equivalent to soft copper wire allowing easy deformation in desired shapes. The SMA generates a large force against the surrounding, during its marten-site to austenite phase transformations. According to the phase transitions and their configurations there are three types of shape memory effects: One-way memory effect, Two-way memory effect, Pseudo-elastic memory effect.

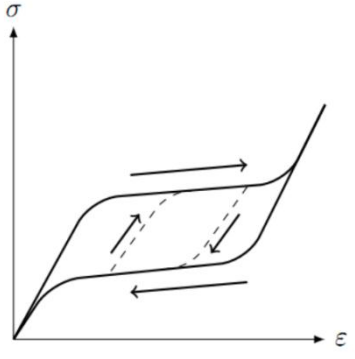

Figure 19: Stress versus Strain of SMA

The source of the unique behaviour of shape memory alloy is the multiphase crystalline structure. The flow of the phase transitions from initial state to final state can be recognized as the hysteresis loading path due to their stress loading. Due to this loading path, SMA said to have "biased stiffness" characteristics. The material will have two different elastic properties with respect to loading: it will be very stiff to comprehensive loading or it will be very flexible to tensile loading. This difference in texture can be found out when the loading is stopped along its hysteresis effect.

Modeling of phase transformation:

The control of SMA is imprecise and difficult because of its hysteresis characteristics. As SMA has two phases and the transformation is within these two phases, it can be modelled as an electron with two state systems [12]. The distribution of electrons in excited phase and normal phase can be described by the Fermi-Dirac statistics. With the same Fermi-Dirac statistics SMA can be modelled considering austenite phase as excited phase of electron and marten-site phase as normal phase of the electron.

When heating the SMA, its phase transfer from marten-site to austenite which can be described with Fermi-Dirac statistics as [12],

$$\xi = \frac{\xi_m}{1+\exp[(T_{fa}-T)/\sigma_a)+K_a\sigma]} \quad \text{----------(5)}$$

Where,

ξ represents a fraction of the austenite phase

ξ_m is the fraction of marten-site phase (before the transformation from marten-site to austenite)

T is the temperature

T_{fa} is the transition temperature from marten-site to austenite

σ_a is an indication of the range of temperature around the transition temperature

σ is the stress

K_a is the stress-curve fitting parameter which is obtained from the loading plateau of the stress-strain characteristic with no change in temperature.

The austenite phase is transferred to marten-site phase, on cooling. It can also be described as Fermi-Dirac statistics as [12],

$$\xi = \frac{\xi_a}{1+\exp[(T_{fm}-T)/\sigma_m)+K_m\sigma]} \quad \text{----------(6)}$$

Where,

ξ is the fraction of the marten-site phase

ξa is the fraction of marten-site phase (before the transformation from austenite to marten-site)

T is the temperature

Tfm is the transition temperature from austenite to marten-site

σm is an indication of the range of temperature around the transition temperature

σ is the stress

Km is the stress-curve fitting parameter which is obtained from the loading plateau of the stress-strain characteristic with no change in temperature.

$$\xi a + \xi m = 1 \text{----------} (7)$$

The sum of mole-fractions of austenite and marten-site phase is 1 at any time of transitions, as SMA is modeled as two component system. Thus, SMA can be modeled as an electron using Fermi-Dirac statistics.

Appendix III

Electrical equivalent of IPMC

The actuator can be modeled as an electrical circuit (more appropriately as an RC circuit) which converts applied electrical voltage into inner current [20].

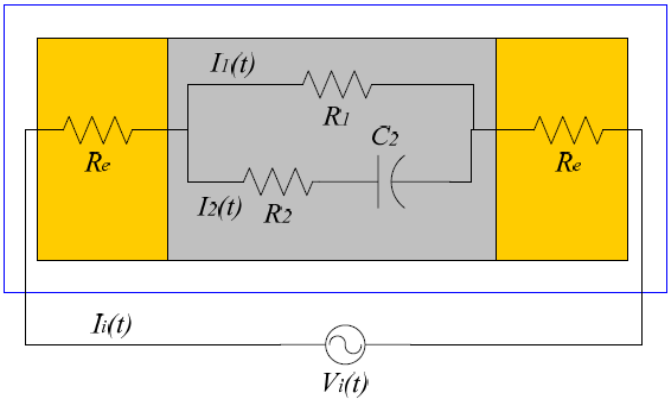

Figure 20: Electrical RC Equivalent of IPMC [20]

According to Kirchhoff's voltage law, we can have:

$$Vi(t) = R_2[Ii(t)-(Vi(t)-2ReIi(t))/R_1]+2ReIi(t)+(1/C_2)\int [Ii(t) - (Vi(t) - 2ReIi(t))/R_1]dt \text{----------} \mathbf{(8)}$$

After applying the Laplace transformation and rearranging the equation and assuming no initial current flow,

$$Qi(s) = [Ii(s)/s] = [s(R_1C_2+R_2C_2)+1][Vi(s)]/[s(R_1R_2C_2+2R_2R€C_2+2R_1R€C_2)+s(R_1+2R€)] \text{----------} \mathbf{(9)}$$

There are two stages from which the IPMC converts the applied electrical supply to mechanical deformation. They are:

1. Nafion 117 (an IPMC) has sodium ions and water molecules. When an electrical supply is applied, when the IPMC is surrounded by water, the hydrated sodium ion moves with four hydrated water molecules to the cathode side which results in the generation bending deformation by the swelling of Nafion 117 at the same side, and it contracts near the anode side.
2. After deformation, the actuator has the potential to recover it, so a self-diffusion is produced which causes the water molecules to flow gradually to the anode side. This reduces the concentration of water molecules at the cathode and the swelling of the actuator at the cathode side is recovered.

The current absorbed by an IPMC actuator induces a mechanical reaction via the redistribution of the inner

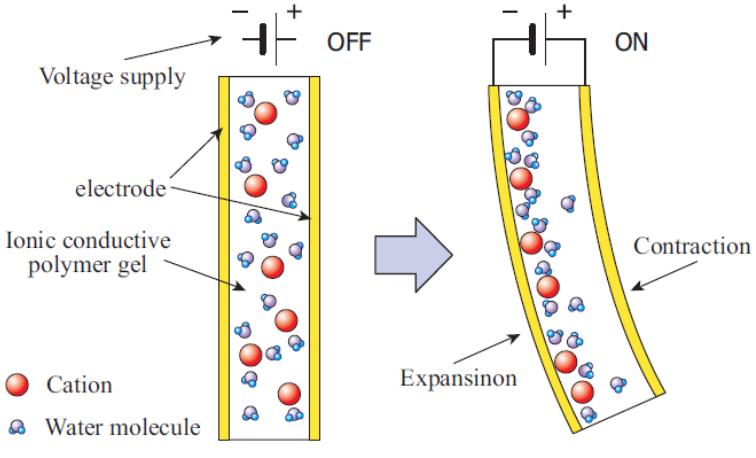

Figure 21: Mechanical Deformation of IPMC [20]

charges/water molecules, resulting in a mechanical bending of the actuator. The dynamic bending displacement, $\delta(t)$ of an IPMC beam is determined by the concentration of water molecules $W(t)$, as follows:

$$\delta(t) = kW(t) = 4kQi(t) \text{----------} \mathbf{(10)}$$

After applying Laplace transformation and substituting Qi(s), $\delta(s)$ can be obtained with respect to Vi(s).

Mechanical deflection

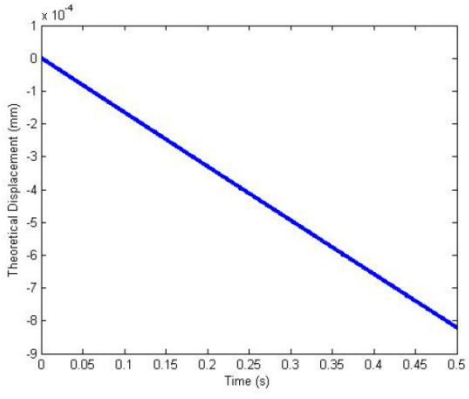

Figure 22: Tip deflection of IPMC

The deformation coefficient *k* is assigned a test value for the IPMC sample. An assumption for an external stimulus to be, *Vi*(t) = 4(t), so that *Vi*(s) = 4/*s*. Applying the inverse Laplace transformation to the obtained $\delta(s)$, $\delta(t)$ can be calculated theoretically with respect to time, which is shown in the figure 22.